Giant monopole resonance strength in ^{28}Si

D. H. Youngblood, H. L. Clark, and Y.-W. Lui
Cyclotron Institute, Texas A&M University, College Station, Texas 77843
(Received 20 October 1997)

The giant resonance region in ^{28}Si was studied with inelastic scattering of 240 MeV α particles at small angles including 0°. The giant resonance peak extended from $E_x = 12$ MeV to 35 MeV and $E0$ strength corresponding to $54 \pm 6\%$ of the isoscalar $E0$ energy weighted sum rule was identified between $E_x = 11-35$ MeV with a centroid of 21.5 ± 0.3 MeV and an rms width of 5.9 ± 0.2 MeV. $E2$ strength corresponding to $32 \pm 5\%$ of the isoscalar $E2$ sum rule was identified with a centroid of $E_x = 19.0 \pm 0.2$ MeV and rms width of 1.7 ± 0.2 MeV. Elastic scattering was measured from $\theta_{\text{c.m.}} = 3°$ to 47° and optical parameters obtained. Inelastic scattering to states at 1.78, 6.88, 10.2, and 11.1 MeV was measured and deformation lengths and L components extracted. [S0556-2813(98)01303-X]

PACS number(s): 24.30.Cz, 25.55.Ci, 27.40.+z

INTRODUCTION

The isoscalar giant monopole resonance (GMR) is of particular interest because its energy is directly related to the compressibility of nuclear matter (K_{nm}) [1]. In the scaling approximation, nuclear compressibility is related [1] to $E_{\text{GMR}} = (m_3/m_1)^{1/2}$, where $m_k = \Sigma (E_n - E_0)^k |\langle 0|r^2|n\rangle|^2$. In order to account for contributions from finite nuclei and extract K_{nm} macroscopic analyses [2] of the GMR require that the energy of the GMR be known in nuclei over a wide range of A. However, until recently, significant monopole strength has been located [2,3] in only a few nuclei with $A < 90$. In recent work [4] using inelastic scattering of 240 MeV α particles at 0° with a new spectrometer and beam analysis system, we obtained much higher peak to background ratios for quadrupole and monopole resonances than previous works and were able to show that no more than 50% of the isoscalar $E0$ energy weighted sum rule (EWSR) is present below $E_x = 25$ MeV in ^{58}Ni. However, in ^{40}Ca we found evidence [5] for $93 \pm 15\%$ of the $E0$ EWSR centered at $E_x = 18.3$ MeV with $(m_3/m_1)^{1/2} = 21.2$ MeV, which is quite consistent with the trend [2] for heavier nuclei.

Lui *et al.* [6] studied ^{28}Si with inelastic scattering of α particles of $E_\alpha \approx 129$ MeV including scattering to 0°, where monopole strength is enhanced and reported 66% of the $E0$ EWSR centered at $E_x = 17.9$ MeV with a width of 4.8 MeV. At this beam energy, the $(\alpha, ^5\text{Li})$ and $(\alpha, ^5\text{He})$ reactions with subsequent decay of the mass five products into an α particle and a nucleon produce broad peaks in the α particle spectrum corresponding to $24 < E_x < 46$ MeV in ^{28}Si. These ''pickup-breakup'' peaks would obscure GMR strength above $E_x \approx 24$ MeV and may hamper determination of the continuum under the giant resonance peaks.

We have studied ^{28}Si using 240 MeV α particles where the ''pickup-breakup'' peaks appear above $E_x = 42$ MeV, well outside of the region where GMR strength is expected. We report here results with excellent peak to continuum ratios taken at small scattering angles including 0°.

EXPERIMENTAL TECHNIQUE AND RESULTS

A beam of 240 MeV α particles from the Texas A&M K500 superconducting cyclotron bombarded a self-supporting natural Si wafer 7.92 mg/cm^2 thick located in the target chamber of the multipole-dipole-multipole spectrometer [7]. Beam was delivered to the spectrometer through a beam analysis system having two bends of 88° and 87° [8]. The beam was limited by slits after the first bend, and the second bend was used for clean up, with slits located so as not to intercept the primary beam. The horizontal acceptance of the spectrometer was 4° and ray tracing was used to reconstruct the scattering angle. The vertical acceptance was set at ±2°. When the spectrometer central angle (θ_{spec}) was set to 0°, the beam passed beside the detector and was stopped on a carbon block inside a Faraday cup behind the detector. For $3.5° < \theta_{\text{spec}} < 6°$, the beam was stopped on an insulated Ta block beside the solid angle defining slits. At larger angles the beam was stopped on a Faraday cup in the target chamber. At $\theta_{\text{spec}} = 0°$, runs with an empty target frame showed α particles uniformly distributed in position at a rate about 1/2000 of that with a target in place.

A new 60 cm long focal plane detector was constructed which covered approximately 55 MeV of excitation. Its principles of operation are similar to the detector described in Ref. [9]. It contains four proportional counters to measure x position at four points along a rays path using the method of charge division, as well as an ionization chamber to provide ΔE and a scintillator to measure total energy and provide a fast timing signal for each ray. The out-of-plane scattering angle ϕ was not measured. To improve the quality of the position spectra, θ for each ray was calculated separately using data from independent wire pairs, and events in disagreement by more than two standard deviations were discarded [9]. Position resolution of approximately 0.9 mm and scattering angle resolution of about 0.09° were obtained. The angle calibration was obtained from an angle spectrum taken with a mask having five openings 0.1° wide spaced 1° apart. The actual spectrometer angle was determined from the kinematic crossover from the elastic scattering off hydrogen (in the ^{12}C target) and ^{12}C inelastic scattering peaks. The calibration procedures are described in detail in Refs. [9] and [10].

Data were taken with ^{12}C, ^{24}Mg, and ^{28}Si targets at the actual field settings used in the experiments. The positions of

 © 1998 The American Physical Society

the 9.641 and 18.350 MeV states [11] in ^{12}C, the 10.18, 18.67, and 20.43 MeV states [12,6] in ^{28}Si, and the 12.86 and 17.36 MeV states [12] in ^{24}Mg were used to obtain momentum calibrations linear in position for each of the spectra. The energies of these known narrow peaks between 9 and 21 MeV were consistently reproduced better than 50 keV.

Giant-resonance data were taken with $\theta_{\rm spec}$ set at 0°, 3.5°, and 5.5° covering the angular range from 0° to 7.5°. The excitation energy range observed was $7<E_x<60$ MeV.

Elastic and inelastic scattering data were taken at spectrometer angles of 3.5° and 5.5° at a different dipole field setting covering the range $-10<E_x<45$ MeV but with the spectrometer acceptance the same as for the giant resonance data. In addition, elastic and inelastic scattering data were taken over the angular range from 2° to 40°, with the vertical acceptance of the spectrometer reduced to $\pm 0.8°$, in order to obtain optical-model parameters.

Each data set was divided into ten angle bins, each corresponding to $\Delta\theta \simeq 0.4°$ using the angle obtained from ray tracing. ϕ is not measured by the detector, so the average angle for each bin was obtained by integrating over the height of the solid angle defining slit and the width of the angle bin. For comparison with theoretical calculations, the data points are plotted at this average angle so that, for example, data from the central angle bin taken with the spectrometer at 0° would be plotted at $\theta_{\rm lab}=1.08°$. By plotting the data versus the average angle, the primary effect of the large solid angle is to fill in deep minima. The phase and cross section maxima are affected only slightly. With the reduced vertical opening [$\pm 0.8°$], the cross section correction to the elastic scattering from averaging over the angle opening was 3% at 2.5° and less than 1% at larger angles except in the minima, when the averaged cross sections were plotted at the average angle determined as described above. This is particularly important for optical model fits because the optical model codes do not take into account averaging over a large vertical opening where the effective angular range for each data point is different.

Cross sections were obtained from the charge collected, target thickness, dead time and known solid angle. The overall dead time of the electronics and computer data acquisition system was measured by passing pulses from a random (in time) pulser into the preamplifiers and through the entire system into the computer. They were checked by comparing the total number of pulses sent to the computer with the number in the spectra. Dead times obtained from the two methods agreed to within 1%. Approximately 16% of events which made it into the computer were discarded because the angles measured in the two sets of horizontal wires did not agree. The cumulative uncertainties in target thickness, solid angle, etc., result in about a $\pm 10\%$ uncertainty in absolute cross sections. The consistency of the current integrator was checked for the elastic scattering data with a monitor detector fixed at 20°.

Angular distributions of the elastic scattering and inelastic scattering exciting the 1.7789 MeV 2^+, 6.8786 MeV 3^-, 10.18 MeV 3^-, and 11.0 MeV ($1^- + 4^+$) states are shown in Figs. 1 and 2. Data points obtained from both the giant

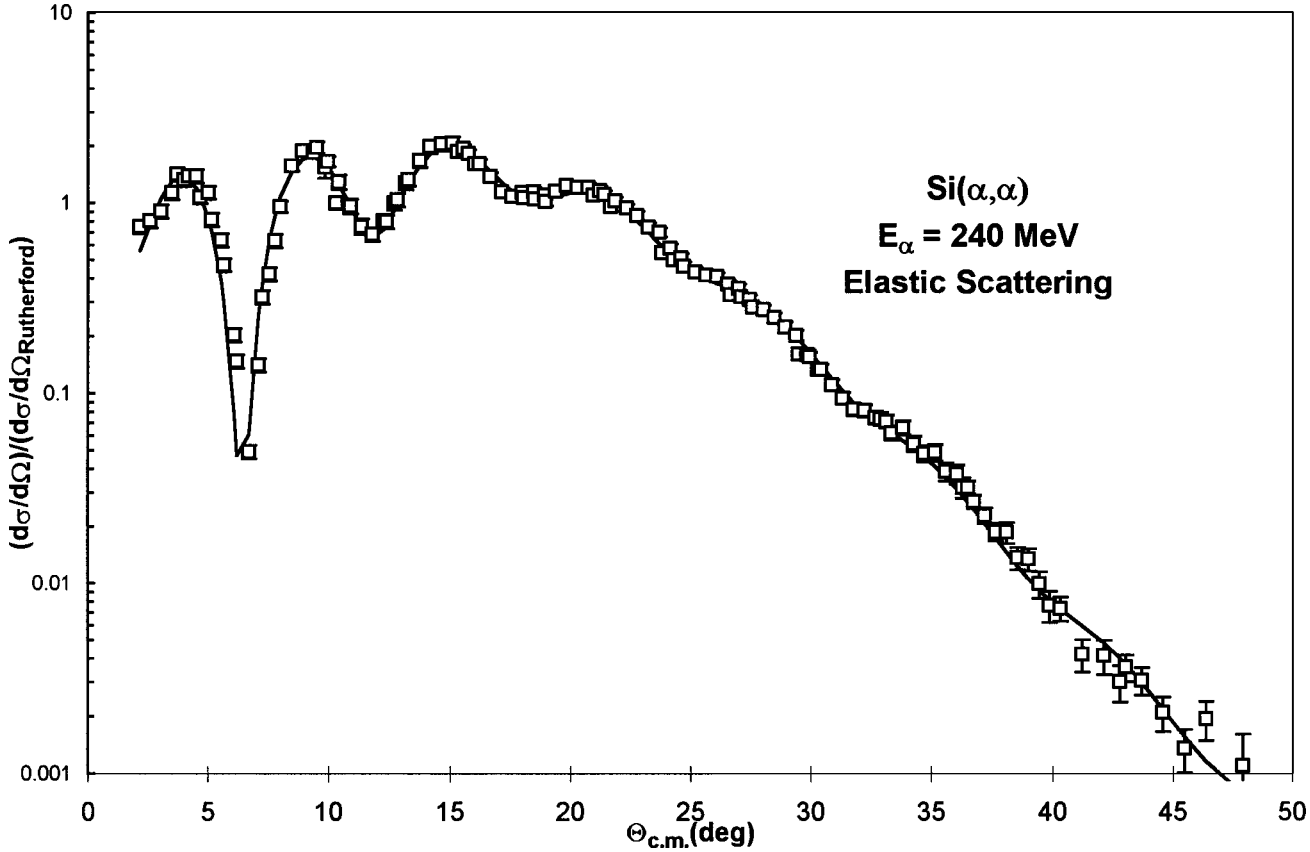

FIG. 1. Angular distribution of the ratio of the differential cross section for elastic scattering to Rutherford scattering for 240 MeV α particles from Si is plotted versus average center-of-mass angle. The solid line shows an optical model calculation with the parameters from Table II. When not shown, statistical errors are smaller than the data points.

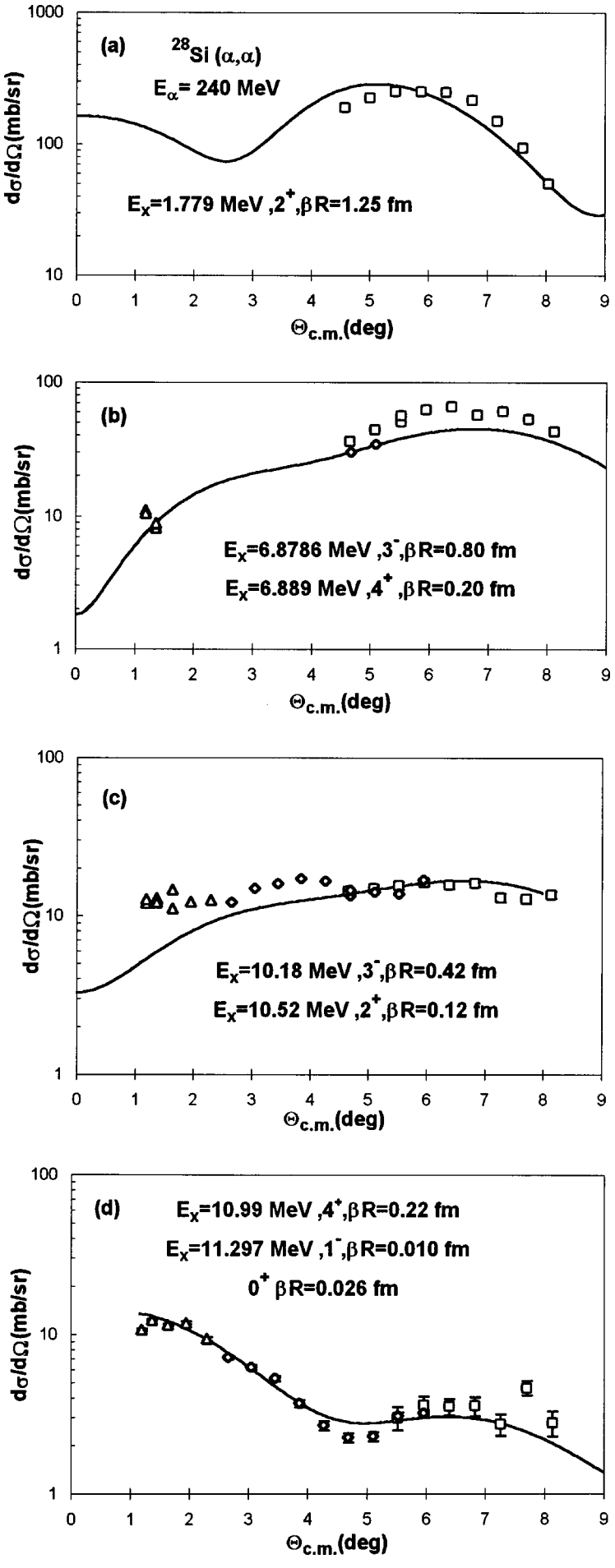

FIG. 2. (a) Angular distribution of the differential cross section for inelastic α scattering to the 1.779 MeV 2^+ state in ^{28}Si plotted versus average center-of-mass angle. The solid line shows an $L=2$ DWBA calculation for $\beta R = 1.25$ fm. (b) Angular distribution of the differential cross section for inelastic α scattering to the 6.879 MeV 3^- and 6.889 MeV states in ^{28}Si plotted versus average center-of-mass angle. The solid line shows a sum of $L=3$ and $L=4$ DWBA calculations for $\beta R=0.80$ and 0.20 fm, respectively. (c) Angular distribution of the differential cross section for inelastic α scattering for a peak corresponding to $E_x=10.20$ MeV in ^{28}Si plotted versus average center-of-mass angle. The solid line shows a sum of $L=3$ and $L=2$ DWBA calculations for $\beta R=0.42$ and 0.12 fm, respectively. (d) Angular distribution of the differential cross section for inelastic α scattering for a peak corresponding to $E_x=11.00$ MeV in ^{28}Si plotted versus average center-of-mass angle. The solid line shows a sum of $L=0$, $L=1$, and $L=4$ DWBA calculations for $\beta R=0.26$, 0.010, and 0.22 fm, respectively. For (a)–(d) the square data points were taken with the elastic data at $\theta_{\text{spec}}=5.5°$. The diamonds and triangles were taken with the giant resonance data at $\theta_{\text{spec}}=3.5°$ and 0°, respectively. When not shown, statistical errors are smaller than the data points. The energies of known states, their multipolarities and the βr used in the fits are shown for each angular distribution. The 0^+ component shown in (d) has not been previously reported.

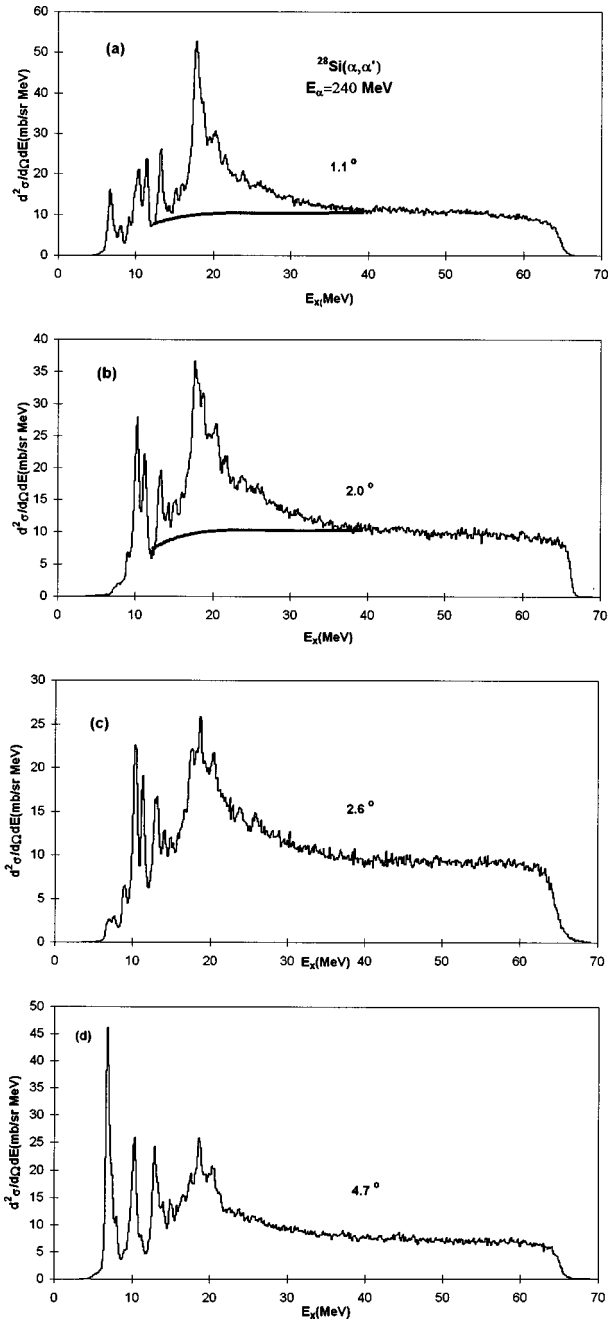

FIG. 3. Spectra obtained for ^{28}Si(α,α') at $E_\alpha=240$ MeV for four angles. The average center-of-mass angles are indicated. Spectra (a) and (b) were taken with the spectrometer at 0°, while spectra (c) and (d) were taken with the spectrometer at 3.5°. The solid line indicates the division between the continuum and the GR peak chosen for the analysis.

resonance and elastic scattering runs are shown for the 10.18 and 11.0 MeV states, and are in good agreement. Giant resonance spectra obtained at several angles are shown in Fig. 3. No background has been subtracted. A very strong narrow peak, previously identified as $L=0$ [6] dominates the spectrum at the smallest angles. The angular distribution of the entire cross section for 15 MeV$<E_x<$25 MeV is shown in Fig. 4. Data points obtained from the giant resonance runs are in excellent agreement with those from elastic scattering runs.

Unlike heavy nuclei where the GQR and GMR are approximately Gaussian peaks, it is clear from previous works [6,12] that the GQR is badly fragmented in ^{28}Si. Further, Lui *et al.* [6] have shown that $E0$ strength in ^{28}Si is also fragmented, so peak fits of the type employed for heavier nuclei are not useful. Thus we have analyzed the data in two different ways. In one method a continuum [illustrated in Fig. 3(a)] is estimated and subtracted, leaving a giant resonance peak. This peak is then divided into several regions and the cross sections summed within each energy interval. The resulting angular distributions are then fit with distorted-wave Born approximation (DWBA) calculations corresponding to several multipolarities. This was the method employed by Lui *et al.* [6]. The angular distributions for the continuum were also summed for the same energy intervals and fit to extract multipole components. Representative angular distributions for different regions of the peak and the continuum are shown in Figs. 5 and 6, respectively. Since monopole strength is strongly forward peaked, a ''spectrum of $E0$ strength'' was generated by subtracting spectra taken at larger angles from those taken at the smallest angles [5,13]. These are shown in Fig. 7(c).

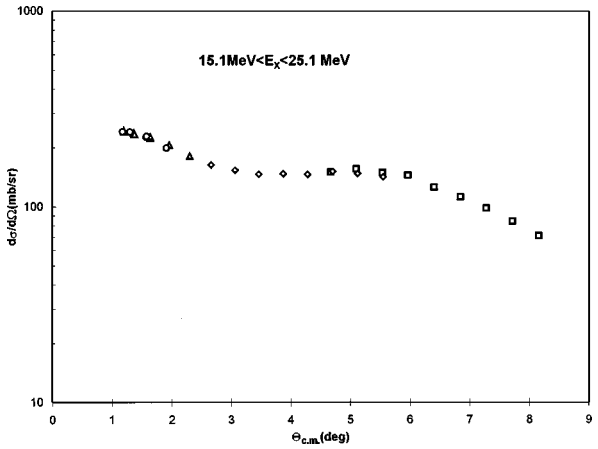

FIG. 4. Angular distribution of the differential cross section obtained for the region $15.1<E_x<25.1$ MeV in ^{28}Si is plotted versus average center-of-mass angle. The data represented by the open squares were taken with the elastic scattering data at a spectrometer angle of 5.5°. The data represented by the open circles and open triangles were taken with the spectrometer at 0° on two different occasions. The data represented by the open diamonds were taken with the spectrometer at 3.5°. When not shown, statistical errors are smaller than the data points.

DWBA AND OPTICAL MODEL ANALYSIS

The transition densities and sum rules for various multipolarities are described thoroughly by Satchler [14]. The GMR has generally been considered a breathing mode oscillation and the corresponding transition density is given by [14]

$$U=-\alpha_0[3\rho+r\,d\rho/dr],$$

where for a state that exhausts the EWSR,

$$\alpha_0^2=2\pi(\hbar^2/m)(A\langle r^2\rangle E_x)^{-1}.$$

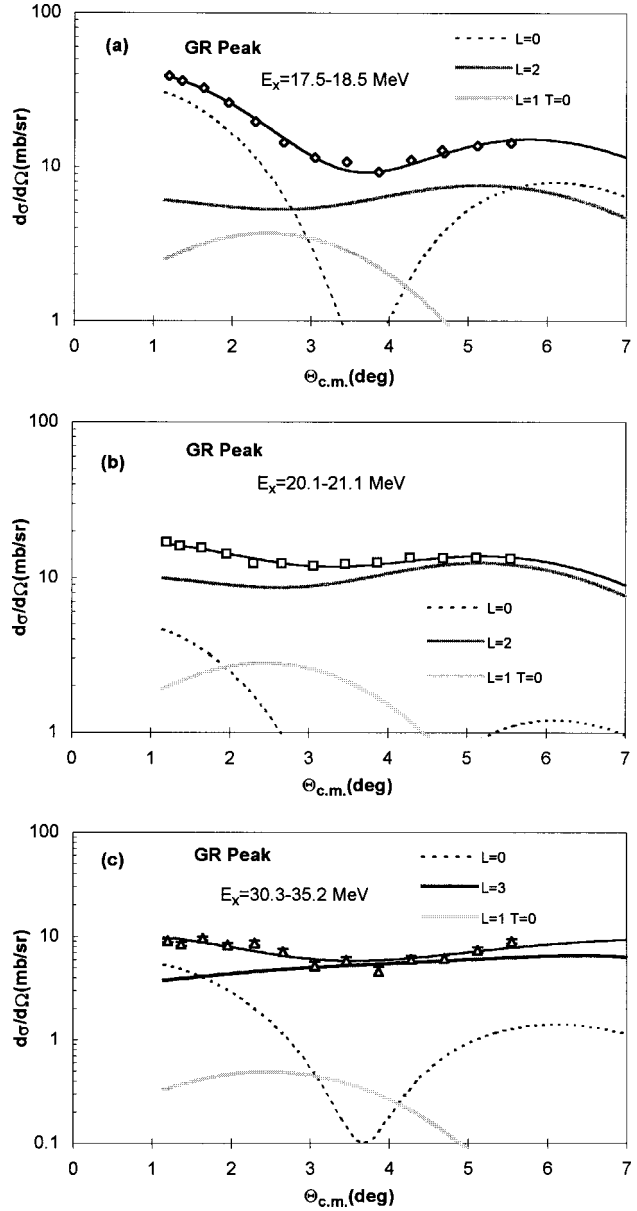

FIG. 5. Angular distributions of the differential cross section for inelastic α scattering for three excitation ranges of the giant resonance peak in ^{28}Si plotted versus average center-of-mass angle. The solid lines show the sum of the distributions for the individual multipolarities. The dashed line shows the $L=0$ component, the wide dark gray shows the $L=2$ component, the light gray shows the $L=1$ $T=0$ component and the wide black line shows the $L=3$ component for each of the regions. The strengths of individual components are plotted in Fig. 9. When not shown, statistical errors are smaller than the data points. (a) shows the data and DWBA for the $E_x=17.5-18.5$ MeV region. (b) shows the data and DWBA for the $E_x=20.1-21.1$ MeV region. (c) shows the data and DWBA for the $E_x=30.3-35.2$ MeV region.

The versions used for other multipoles in this work are given in Ref. [5].

Inelastic α scattering to collective states has been analyzed using either the deformed potential model or the folding model. Beene *et al.* [15] have shown that a consistent agreement between electromagnetic transition strengths and those measured with light and heavy ion inelastic scattering for low lying 2^+ and 3^- states can only be obtained using

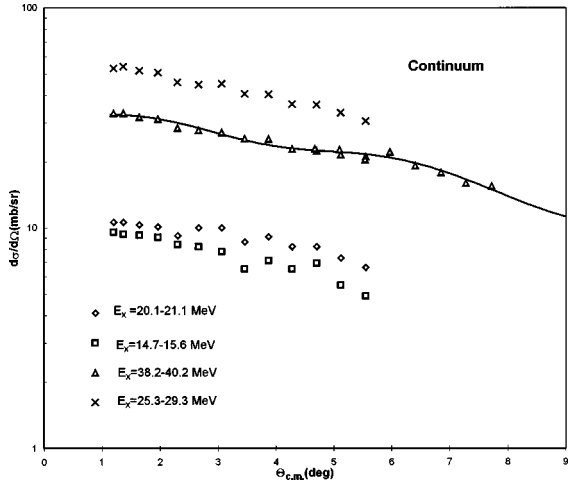

FIG. 6. Angular distribution of the differential cross section for inelastic α scattering for four excitation ranges of the continuum in ^{28}Si plotted versus average center-of-mass angle. The solid line shows DWBA calculations for a sum of multipolarities for the fit to one of the distributions. The multipole components are shown in Fig. 9. Statistical errors are smaller than the data points.

the folding model. Recently Satchler and Khoa [16], analyzing a 240 MeV α study of ^{58}Ni, compared results obtained using the deformed potential model, single folding using a Gaussian α-nucleon force with and without density dependence, and double folding using the BDM3Y1 nucleon-nucleon force which includes density dependence. Their conclusion was that each of the folding calculations gave very similar 0° cross sections for the GMR, and fit the data for the 4.475 MeV 3^- state using the electromagnetic $B(E3)$ value. Deformed potential calculations required a $B(E3)$ value about a factor of 2 below the electromagnetic value to fit the experimental data for the 4.475 MeV state. However, if the potential deformation length was set equal to the mass deformation length ($\alpha_m c=\alpha_p R_p$) for the GMR, then nearly the same 0° cross section was obtained with the deformed potential as with the folding models. Similar results were obtained in our recent study of ^{40}Ca [5]. The strengths and angular distributions obtained for the GMR with the deformed potential and folding models were virtually identical. Thus in this study we present only the deformed potential analysis.

Distorted-wave Born approximation and optical-model calculations were carried out with the code PTOLEMY [17]. Input parameters for PTOLEMY were modified [18] to obtain a relativistic kinematically correct calculation. The amplitudes of the transition densities for the various multipoles obtained from the expressions in Ref. [5] for 100% of the respective sum rules are given in Table I. Radial moments for ^{28}Si were obtained by numerical integration of the Fermi mass distribution assuming $c=3.155$ fm and $a=0.523$ [19].

Optical-model parameters were obtained for ^{28}Si by fitting the elastic scattering, and the resulting fits are shown in Fig. 1. The parameters are listed in Table II. DWBA calculations using the deformed potential model were carried out for the states shown in Fig. 2 and are shown superimposed on the data. The multipolarities and βR values resulting in the best fits are shown on the figures. Except for the $E_x=1.779$ MeV 2^+ state, the other three groups were a com-

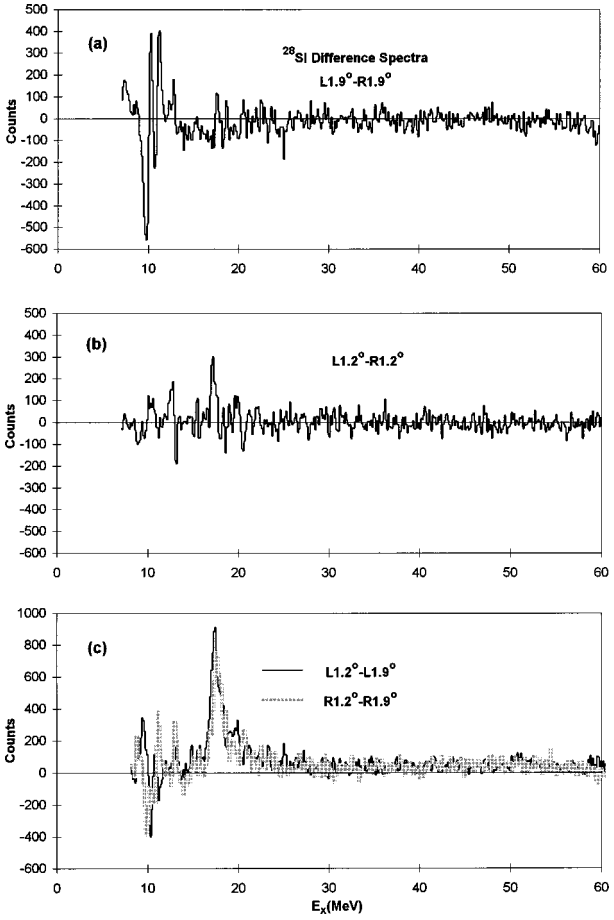

FIG. 7. Difference spectra obtained as described in the text. (a) The result of subtracting a spectrum for $\theta_{\rm avg}$=L1.9° from that taken at $\theta_{\rm avg}$=R1.9°. (b) The result of subtracting a spectrum for center-of-mass angle $\theta_{\rm avg}$=L1.2° from that taken at $\theta_{\rm avg}$=R1.2°. (c) The black line shows the result of subtracting the spectrum taken at $\theta_{\rm avg}$=L1.9° from the spectrum taken at $\theta_{\rm avg}$=L1.2°. The gray line shows the result of subtracting the spectrum taken at $\theta_{\rm avg}$=R1.9° from the spectrum taken at $\theta_{\rm avg}$=R1.2°. L in front of the angle indicates the angle is on the left side of the beam and R indicates the angle is on the right side of the beam.

bination of more than one known state. Good fits were obtained with multipolarities known to be present and βR values close to those obtained by van der Borg [12] with the particular exception of the 11.1 MeV group, which in addition to the expected 4^+ and 1^- components, required a sizable 0° component (corresponding to 2.2% of the $E0$ EWSR) because of the rapid rise in the cross section at small angles. The $B(E3)$ value obtained for the 6.879 MeV 3^- state with the deformed potential is about a factor of 2 lower than the electromagnetic value, but in agreement with other α scattering measurements analyzed with the deformed potential model. A calculation for the 10.18 MeV state with both the expected 3^- and 2^+ components fits the data well beyond about 4°. At smaller angles it is likely that other weak and unresolved states are contributing to the yield.

TABLE I. Deformation lengths for 100% of the respective sum rules in ^{28}Si.

Isoscalar	Deformation Length (fm)	E_x (MeV)
$L=0$	$\alpha_0 c=0.726$	18.0
$L=1$	$\beta_1 c=0.425$	20.0
$L=2$	$\beta_2 c=1.353$	18.0
$L=3$	$\beta_3 c=2.144$	18.0
$L=4$	$\beta_4 c=3.278$	18.0
Isovector		
$L=1$	$B(E1)=0.05197\ e^2$b	20.0

TABLE II. Optical-model parameters obtained from fits to elastic scattering.

V (MeV)	R (fm)	a (fm)	W (MeV)	R_i (fm)	a_i (fm)	R_c (fm)
96.48	3.586	0.811	22.85	4.697	0.688	4.446

Angular distributions for the different multipoles that might contribute between E_x=10–35 MeV are shown in Fig. 8 for 100% of the respective EWSR. The striking characteristic of monopole strength is the strong peaking of the cross section at 0° where the monopole would be by far the largest contribution. Thus GMR strength would be characterized by strong forward peaking in the angular distribution. The isovector giant dipole resonance (GDR) is also forward peaked (excited only by Coulomb excitation in ^{28}Si), but is much weaker than the other multipolarities and has no impact on this analysis.

DISCUSSION

Fits to the angular distributions of the continuum and the peak regions were carried out with a sum of isoscalar 0^+, 1^-, 2^+, and 3^- strengths. The GDR cross section would be negligible and was not added in. The strengths were varied to minimize χ^2. Over the angle range of the data, angular distributions for $L\geqslant 3$ are very similar and could not be distin-

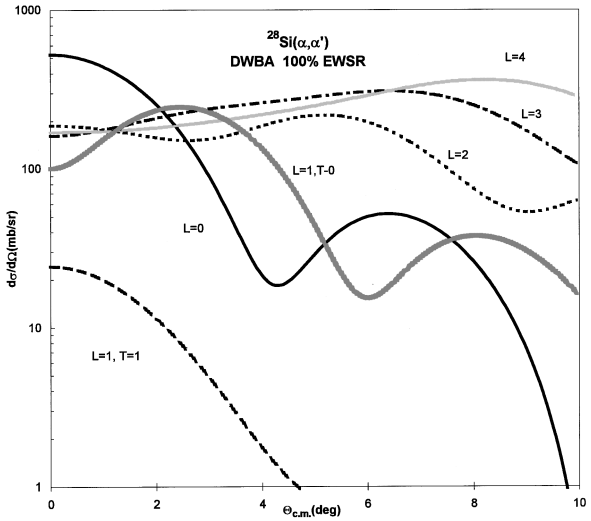

FIG. 8. Angular distributions of the differential cross sections for various multipoles for 100% of the respective sum rules using deformation lengths from Table I.

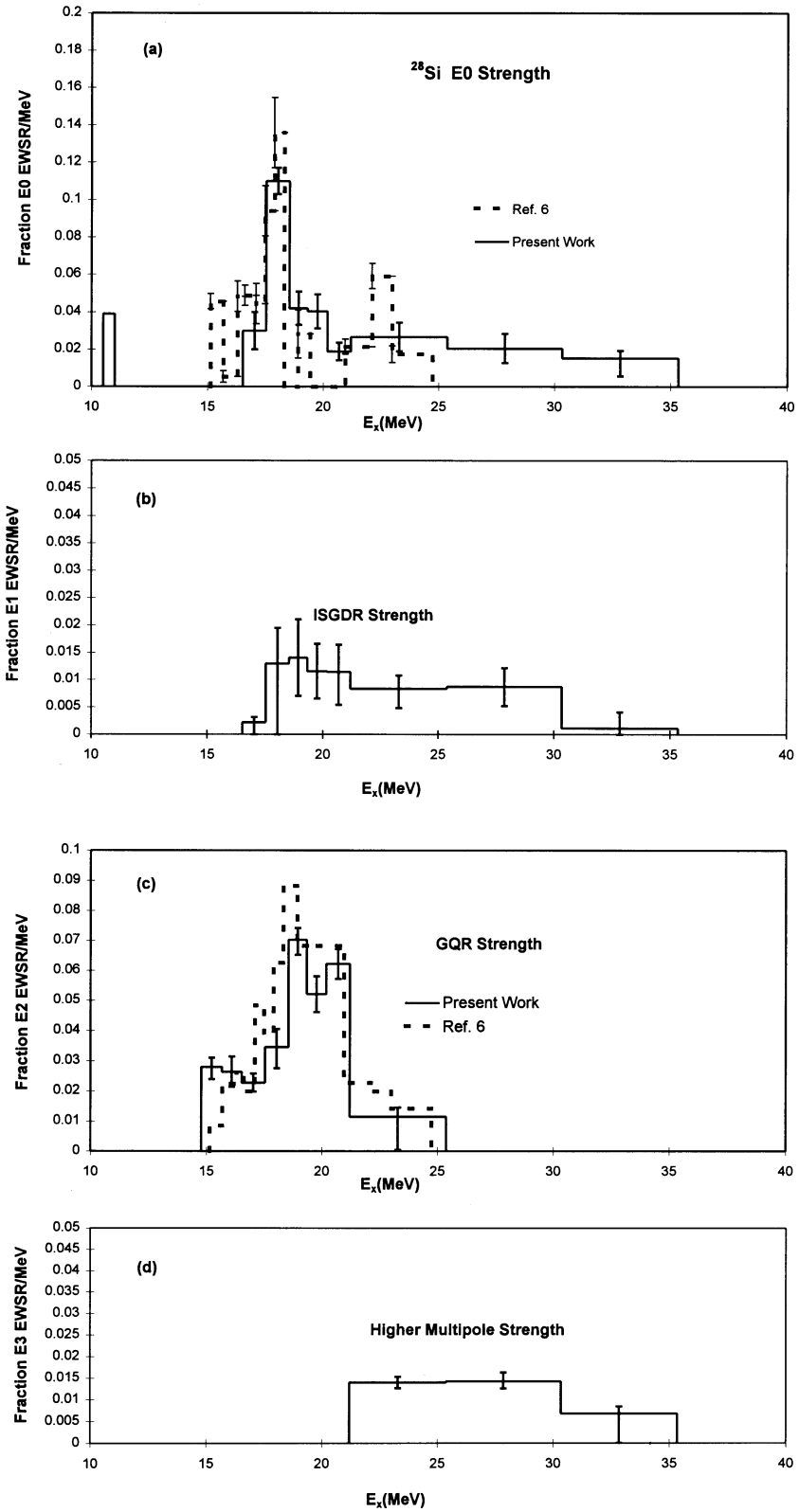

FIG. 9. (a) The dashed line shows the fraction of the $E0$ EWSR in the ^{28}Si giant resonance peak obtained from the results of Ref. [6] as described in the text. The solid line shows the fraction of the $E0$ EWSR obtained for the GR peak in this work. The error bars represent the uncertainty due to the fitting of the angular distributions. (b) The solid line shows the fraction of the isoscalar $E1$ EWSR obtained from the fits to the angular distributions of the cross section in the peak. The error bars represent the uncertainty due to the fitting of the angular distributions. (c) The solid line shows the fraction of the isoscalar $E2$ EWSR obtained from the fits to the angular distributions of the cross section in the peak. The dashed line shows the distribution from Ref. [6]. The error bars represent the uncertainty due to the fitting of the angular distributions. (d) The solid line shows the fraction of the HEOR EWSR obtained from the fits to the angular distributions of the cross section in the peak assuming all the strength fit as $L=3$ belongs to the HEOR, though the fits cannot distinguish between $L\geqslant 3$. The error bars represent the uncertainty due to the fitting of the angular distributions.

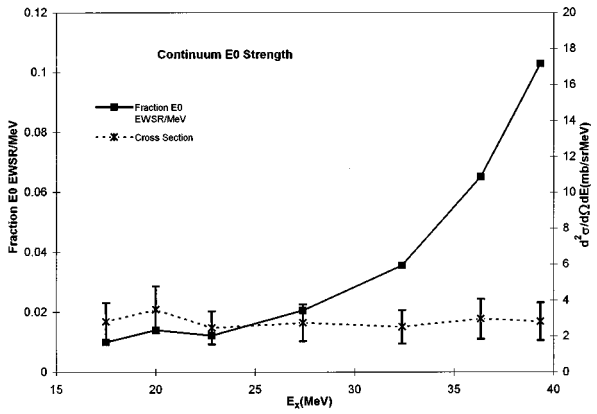

FIG. 10. The dashed line shows the cross section/MeV at $\theta_{\text{c.m.}} = 1.1°$ for $E0$ excitation in the continuum obtained from fits to the angular distributions for regions centered at the data points. The solid line shows the fraction of the $E0$ EWSR extracted from this cross section. The error bars show the uncertainty in the $E0$ component obtained from the fits.

guished. Figure 5 shows angular distributions obtained for three excitation regions in the giant resonance (GR) peak where differing multipolarities dominate as well as DWBA calculations for each component of the fits. The EWSR fractions for each of the components as well as the errors for each component are shown in Fig. 9. A sample fit to one of the continuum regions is shown in Fig. 6. The $E0$ strengths obtained for the peak, the continuum, and for the total are shown in Figs. 9, 10, and 11 respectively and summarized for broad energy ranges in Table III. The $E0$ distribution obtained is in excellent agreement with the (adjusted—see below) results from Lui *et al.* [6] up to $E_x = 25$ MeV, the upper limit of their work. Energy moments of the $E0$ distribution are given in Table IV. Also shown in Fig. 9 are the distributions of $T=0$ 1^-, 2^+, and 3^- strengths required to fit the angular distributions for the peaks. The 2^+ strength is peaked at about $E_x = 19.0$ MeV and contains 32 ± 6 % of the isoscalar $E2$ EWSR. This is in excellent agreement with Lui *et al.* [6] who reported 34 ± 6% of the $E2$ EWSR centered at 19 MeV. The 1^- strength is fairly weak and has large uncertainties, but appears to be distributed almost uniformly over the region $E_x = 15$ to $E_x = 35$ MeV. This strength corresponds to a total of 13 ± 4% of the isoscalar dipole sum rule. Lui *et al.* did not report any $E1$ strength. It can be seen in Fig. 5 that there are obviously strong $L=0$ and $L=2$ components in the angular distributions, however, the $L=1$ strength is needed primarily to reduce the first minimum in the $L=0$ angular distribution. This is why the errors on $E1$ strength are large. However, while the peak cross section for

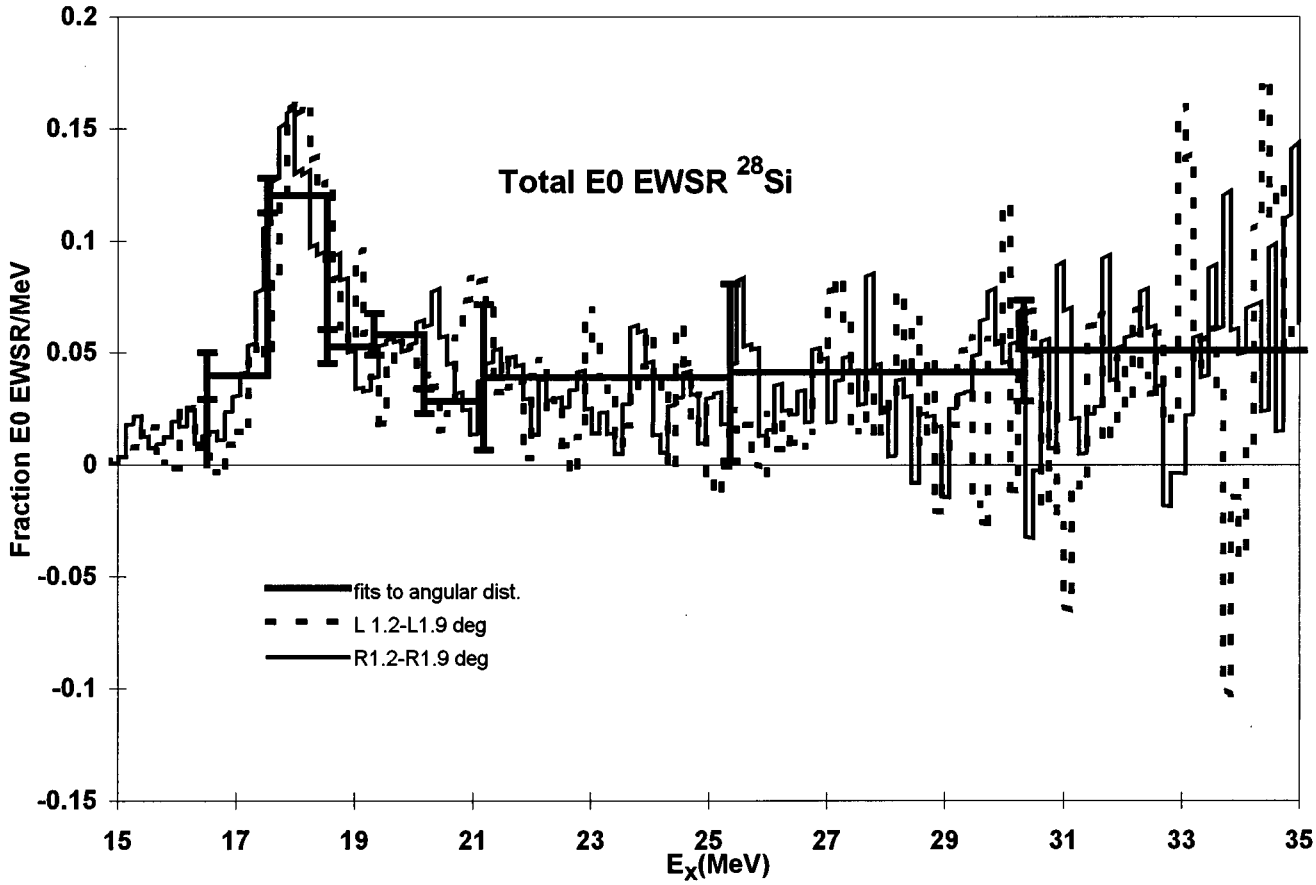

FIG. 11. The thicker dark line shows the fraction of the $E0$ EWSR obtained from fits to the angular distributions of regions of excitation of the entire yield for ^{28}Si. The error bars represent the uncertainty due to the fitting of the angular distributions. The thin dark line shows the fraction of the $E0$ EWSR obtained from the difference spectrum from the left side of the beam and the dashed line shows that obtained from the right side of the beam.

TABLE III. Monopole-resonance sum-rule strengths for ^{28}Si obtained from difference spectra and from fits. Errors for difference spectra results are statistical only. Systematic errors due to angle calibration discussed in text are shown in parenthesis. Errors given for peak fits are the range for which χ^2 increases by a factor of 2.

	Difference spectra		Fits	
E_x Range (MeV)	L 1.2°–1.9° %$E0$ EWSR	R 1.2°–1.9° %$E0$ EWSR	Peak+cont. %$E0$ EWSR	Peak only %$E0$ EWSR
15.0–20.0	30.4±1.1(3.5)	27.5±1.4(4.6)	25±3	21±2
20.0–30.0	31.9±3.1(9.8)	30.7±3.9(12)	37±7	23±2
30.0–35.0	24.6±5.2(9.7)	20.1±6.0(12)	26±6	7.7±2.0
15.0–35.0	89±6(24)	79±8(29)	88±10	52±6
35.0–41.0	75±14(27)	74±17(32)	54±16	
10.7–11.5				2.2±0.7

$E0$ strength is virtually independent of optical parameters and model, the depth of the valley in the first minimum is sensitive to the parameters, thus the total errors on $E1$ strength may be considerably larger than those extracted from the fit. The amount of $E1$ strength has little effect on the other multipoles. $L \geqslant 3$ strength is seen only at the higher energies ($E_x > 21$ MeV) and, if attributed to $L=3$, corresponds to about 17±5% of the isoscalar $E3$ EWSR.

Lui *et al.* [6] obtained ^{28}Si $E0$ strengths using both the breathing mode form factor and the Satchler version 2 form factor. They used a square well approximation in arriving at the sum rule strength and assumed the mass and potential deformation parameters (α_0) were the same, whereas in this work the deformation lengths ($\alpha_0 c$) were taken to be the same. Therefore we did DWBA calculations for the 129 MeV data of Lui *et al.* using their optical potentials and the sum rule value for $L=0$ from Table I and renormalized their strengths accordingly. The resulting $E0$ strength distribution from the 129 MeV data is compared to the distribution obtained in this work by fitting angular distributions of slices of the peak (after continuum subtraction) in Fig. 9(a). The integrated $E0$ strengths obtained for two different energy regions are also shown in Table V. It can be seen that the 240 and 129 MeV results, analyzed with the same transition potential and sum rule assumptions, are in excellent agreement. Our values are considerably below (a factor of 2) the results they report using the version 2 form factor, and above their results with the breathing mode form factor. See Ref. [5] for a discussion of differences resulting from the square well assumption and from equating the deformation parameters for mass and potential oscillations rather than equating the deformation lengths. The energy moments of the $E0$ strength obtained in this work are considerably higher than those of Ref. [6] due to the much wider excitation range explored in this work.

Between $E_x = 15-35$ MeV a total of 52±6% of the $E0$ EWSR is present in the GR peak. The fits would suggest that an additional 36% of the $E0$ EWSR is located in the continuum under the peak. The distribution of the continuum $E0$ cross section and strengths are shown in Fig. 10. As can be seen the cross section/MeV attributable to $E0$ strength is essentially constant from $E_x = 17$ to $E_x = 39$ MeV but the resulting $E0$ EWSR strength increases dramatically at higher excitation. The reason for this can be seen in Fig. 12 where the predicted 0° cross section for monopole excitation with 100% of the $E0$ EWSR is plotted versus excitation energy. The expected cross section drops rapidly with excitation energy. Thus nearly half of the continuum contribution to the $E0$ strength would be from the highest energy interval alone. The angular distributions from the different energy regions of the continuum (Fig. 6) are all very similar and generally decrease with angle. Some $E0$ component is required in a fit with various multipoles to reproduce such an angular distribution. However, it is also possible that there is some other reaction mechanism contributing to the continuum which peaks at small angles and slowly decreases with angle. This experiment cannot distinguish these two possibilities.

Since the $E0$ angular distribution is strongly peaked near 0°, and the angular distributions for the other multipolarities are nearly flat below 2°, ''spectra of $E0$ strength'' have been obtained [17,5] by subtracting data taken at larger angles from data taken at 0°. With the spectrometer at 0°, there are spectra at similar angles on opposite sides of the beam that should be identical. As the spectrometer was actually at 0.3° relative to the beam, spectra taken at the same angles with respect to the beam should not have the same slit scattering (from slit edges at in plane angles of 2.3° and −1.7° relative to the beam). Difference spectra obtained by subtracting a spectrum taken at center-of-mass angle $\theta_{\rm avg} = +1.9°$ ($\theta_{\rm avg} = +1.2°$) from a spectrum taken at $\theta_{\rm avg} = -1.9°$ ($\theta_{\rm avg} = -1.2°$) are shown in Figs. 7(a) and 7(b). The resulting spectra are nearly 0 above $E_x = 20$ MeV. Below $E_x = 11$ MeV there are major excursions in yield caused by minor differences in energy calibration from a nonlinearity in the detector which results in sharp peaks not exactly lining up in different spectra.

Difference spectra obtained by subtracting spectra corresponding to an angle cut near the edge of the slit ($\theta_{\rm lab} = 1.7°$) from spectra taken near the center ($\theta = 0°$) are shown in Fig. 7(c) for two different sets of angle pairs. They are very similar and above the peak region ($E_x > 25$ MeV) agree within statistics. The difference spectra were converted to cross section and then adjusted to a 0° cross section using the DWBA predictions for the GMR, correcting the overall cross section for the GQR contribution. ''Spectra'' of the ''fraction of the $E0$ EWSR'' as a function of E_x were calculated by dividing the spectra of Fig. 7(c) by the DWBA prediction for 100% of the $E0$ EWSR. This is shown in Fig.

TABLE IV. Monopole-resonance parameters for ^{28}Si for 15 MeV$<E_x<$35 MeV.

	Difference spectra		Peak analysis[a]
	L 1.2°–1.9°	R 1.2°–1.9°	
$E_{\rm avg}$ (MeV)	23.5±0.4	23.5±0.3	21.5±0.3
$(m_1/m_{-1})^{1/2}$ (MeV)	22.7±0.3	22.8±0.3	20.7±0.2
$(m_3/m_1)^{1/2}$ (MeV)	26.0±0.5	25.8±0.5	23.7±0.3
rms width (MeV)	6.1±0.1	5.9±0.1	5.9±0.2

[a]Includes $E_x=11.1$ MeV $E0$ strength.

11. Here it can be seen that the small cross section above $E_x=25$ MeV contributes significantly to sum rule strength. The large fluctuations at the higher excitation energies are statistical. In addition to the uncertainty in the absolute cross section, a source of uncertainty that is of particular importance for the subtracted spectra is the relative solid angles for each of the spectra determined from software cuts on θ. From the angle calibrations, we estimate that the relative solid angles are uncertain by ±2.5% between the 1.2° spectrum and the 1.9° spectrum. The uncertainties in $E0$ strengths caused by this are shown in Table III as systematic errors.

The sum rule strengths (m_1) obtained for three excitation regions are listed in Table III. The centroid energies, as well as $(m_1/m_{-1})^{1/2}$, $(m_2/m_0)^{1/2}$, and $(m_3/m_1)^{1/2}$ obtained from the two difference spectra are given in Table IV. The errors shown are statistical only. The total strength seen in the two spectra (89±6 and 79±8 % of the $E0$ EWSR) agrees within statistical errors. With the ±24% systematic uncertainty in $E0$ EWSR strength for the subtracted spectra, the total $E0$ strength obtained with these assumptions from the difference spectra is consistent with 100% of the $E0$ EWSR. Except for the region $12.2<E_x<20.0$ MeV, the $E0$ strengths in the two spectra agree within statistics. The values obtained for the centroids $(m_1/m_{-1})^{1/2}$ and $(m_3/m_1)^{1/2}$ obtained from the two spectra also agree within statistics.

Since $E0$ strength distributions were obtained both from fitting angular distributions (a more stringent requirement) and from difference spectra (essentially a two point angular distribution), the results can be compared. The $E0$ strength distribution obtained by fitting the angular distributions of the peak and the continuum is compared with those obtained from the difference spectra in Fig. 11 and Table III. It can be seen that they generally agree within statistical and fitting errors, suggesting that the systematic error from uncertainty in bin width (which affects only the difference spectra) may be overestimated. The difference spectra provide much better definition of the distribution by mapping the distribution in 1 channel width bins.

TABLE V. Comparison of present experiment with analysis of data from Ref. [6] as discussed in the text.

E_x range (MeV)	%$E0$ EWSR	
	Present experiment	Ref. [6]
15.0–20.0	19±2	20±4
20.0–25.0	11±3	11±2

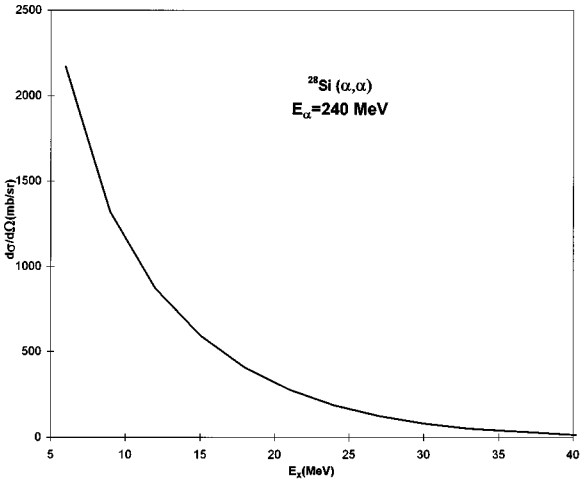

FIG. 12. The solid line shows the 0° $E0$ cross section for 100% of the $E0$ EWSR in ^{28}Si as a function of excitation energy.

CONCLUSIONS

The excitation region from $E_x=10-60$ MeV in ^{28}Si has been studied with 240 MeV α particles at small angles including 0°. At this beam energy the spectra are free of contamination from particle break-up peaks up to $E_x=42$ MeV, increasing the sensitivity to giant resonance strength compared to experiments at lower bombarding energies. The similarity of spectra measured at symmetrical angles on either side of the beam, but not symmetrical relative to the experimental setup, suggests that the experimental background is negligible. The strongest component of the GMR (a peak at $E_x=18.1$ MeV with a width of 0.61 MeV containing approximately 14% of the $E0$ EWSR) has a peak to continuum ratio over 4 at $\theta=0°$, and is seen as a true ''giant resonance'' in the spectrum. A comparison of $E0$ strength extracted from difference spectra is shown to agree with $E0$ strength obtained from fitting angular distributions with a sum of multipoles.

The giant resonance peak extends up to $E_x\approx35$ MeV, well above the region explored in previous experiments. Between $E_x=11-35$ MeV, 54±6% of the $E0$ EWSR was found with an average energy of 21.5±0.3 MeV. A similar analysis suggests that an additional 36±10% of the $E0$ EWSR may be present in the continuum in the same energy region. However, the angular distributions of the continuum are featureless and some or all of the apparent $E0$ strength in the continuum may be due to other mechanisms (unidentified) which produce slightly forward peaked angular distributions. The relatively small but nearly constant cross section in the subtracted spectra [Fig. 7(c)] between $E_x=35-41$ MeV (above $E_x=42$ MeV ^{5}Li breakup would contribute) corresponds to 75% of the $E0$ EWSR, also strongly suggesting that a mechanism besides multipole excitation is present.

Another uncertainty is that of the cross section calculated with DWBA. Two works [5,16] have explored the effects of different types of calculation (deformed potential, single and double folding) and found little difference in the predicted cross section for the GMR. However, the same breathing mode transition density was used for all the calculations, in

part because Hartree-Fock calculations in heavier nuclei give similar transition densities for the GMR in heavier nuclei. If instead one assumes the GMR is a surface oscillation as described by Satchler's [20] version 2 transition density, the predicted cross section for the GMR in ^{28}Si is reduced by a factor of 1.98, and the $E0$ strength observed in the GR peak in this work would correspond to 100% of the EWSR. Thus it is possible that all of the $E0$ strength in ^{28}Si has been located. To clarify this, additional information is needed regarding the monopole transition density in ^{28}Si.

ACKNOWLEDGMENTS

This work was supported in part by the U.S. Department of Energy under Grant No. DE-FG03-93ER40773 and by The Robert A. Welch Foundation.

[1] J. P. Blaizot, Phys. Rep. **64**, 171 (1980).
[2] S. Shlomo and D. H. Youngblood, Phys. Rev. C **47**, 529 (1993).
[3] H. Dennert, E. Aschenauer, W. Eyrich, A. Lehmann, M. Moosburger, N. Scholz, H. Wirth, H. J. Gils, H. Rebel, and S. Zagromski, Phys. Rev. C **52**, 3195 (1995).
[4] D. H. Youngblood, H. L. Clark, and Y.-W. Lui, Phys. Rev. Lett. **76**, 1429 (1996).
[5] D. H. Youngblood, Y.-W. Lui, and H. L. Clark, Phys. Rev. C **55**, 2811 (1997).
[6] Y.-W. Lui, J. D. Bronson, D. H. Youngblood, and Y. Toba, Phys. Rev. C **31**, 1641 (1985).
[7] D. M. Pringle, W. N. Catford, J. S. Winfield, D. G. Lewis, N. A. Jelley, K. W. Allen, and J. H. Coupland, Nucl. Instrum. Methods Phys. Res. A **245**, 230 (1986).
[8] D. H. Youngblood and J. D. Bronson, Nucl. Instrum. Methods Phys. Res. A **361**, 37 (1995).
[9] D. H. Youngblood, Y.-W. Lui, H. L. Clark, P. Oliver, and G. Simler, Nucl. Instrum. Methods Phys. Res. A **361**, 539 (1995).
[10] H. L. Clark, Y.-W. Lui, and D. H. Youngblood, Nucl. Phys. **A589**, 416 (1995).
[11] F. Ajzenberg-Selove, Nucl. Phys. **A506**, 1 (1990).
[12] K. van der Borg, M. N. Harakeh, and A. van der Woude, Nucl. Phys. **A365**, 243 (1981).
[13] S. Brandenburg, R. De Leo, A. G. Drentje, M. N. Harakeh, H. Sakai, and A. van der Woude, Phys. Lett. **130B**, 9 (1983).
[14] G. R. Satchler, Nucl. Phys. **A472**, 215 (1987).
[15] J. R. Beene, D. J. Horen, and G. R. Satchler, Phys. Lett. B **344**, 67 (1995).
[16] G. R. Satchler and Dao T. Khoa, Phys. Rev. C **55**, 285 (1997).
[17] M. Rhoades-Brown, M. H. Macfarlane, and S. C. Pieper, Phys. Rev. C **21**, 2417 (1980); M. H. Macfarlane and S. C. Pieper, Argonne National Laboratory Report No. ANL-76-11, Rev. 1, 1978 (unpublished).
[18] G. R. Satchler, Nucl. Phys. **A540**, 533 (1992).
[19] G. Fricke, C. Bernhardt, K. Heilig, L. A. Schaller, L. Schellenberg, E. B. Shera, and C. W. DeJager, At. Data Nucl. Data Tables **60**, 177 (1995).
[20] G. R. Satchler, Part. Nuclei **5**, 105 (1973).